

Nanoscale

Accepted Manuscript



This is an *Accepted Manuscript*, which has been through the Royal Society of Chemistry peer review process and has been accepted for publication.

Accepted Manuscripts are published online shortly after acceptance, before technical editing, formatting and proof reading. Using this free service, authors can make their results available to the community, in citable form, before we publish the edited article. We will replace this *Accepted Manuscript* with the edited and formatted *Advance Article* as soon as it is available.

You can find more information about *Accepted Manuscripts* in the [Information for Authors](#).

Please note that technical editing may introduce minor changes to the text and/or graphics, which may alter content. The journal's standard [Terms & Conditions](#) and the [Ethical guidelines](#) still apply. In no event shall the Royal Society of Chemistry be held responsible for any errors or omissions in this *Accepted Manuscript* or any consequences arising from the use of any information it contains.

Cite this: DOI: 10.1039/c0xx00000x

www.rsc.org/xxxxxx

ARTICLE TYPE

Direct Evidence of Plasmon Enhancement on Photocatalytic Hydrogen Generation over Au/Pt-Decorated TiO₂ Nanofibers

Zhenyi Zhang,^{a,b} Anran Li,^b Shao-Wen Cao,^b Michel Bosman,^c Shuzhou Li,^b and Can Xue^{*b}*Received (in XXX, XXX) Xth XXXXXXXXX 20XX, Accepted Xth XXXXXXXXX 20XX*

DOI: 10.1039/b000000x

Direct evidence of plasmon-enhanced H₂ generation is observed in photocatalytic water reduction by using TiO₂ electrospun nanofibers co-decorated with Au and Pt nanoparticles through dual-beam irradiation. The Au/Pt/TiO₂ nanofibers exhibit certain activity for H₂ generation under a single irradiation at 420 nm that excites the defect/impurity states of TiO₂. Significantly, when a secondary irradiation at 550 nm is introduced to simultaneously excite Au SPR, we observed 2.5 times higher activity for H₂ generation. Further investigations by finely controlling the irradiation wavelengths reveal that the enhancement factor on the photocatalytic activity for H₂ generation is directly correlated with the plasmon absorption band of the Au nanoparticles in the Au/Pt/TiO₂ nanofibers. The control experiments with different sacrificial agents suggest that the hot plasmonic electrons of Au are responsible to the enhanced photocatalytic activity that can be magnified when TiO₂ is simultaneously excited.

Introduction

In the past decade, semiconductor metal oxides have been widely used as highly stable photocatalysts for solar energy conversion to solve the problems of worldwide energy crisis and environmental pollution.¹ Due to the limited visible light absorption of most metal oxides, plasmonic gold nanoparticles (NPs) have been extensively used to decorate metal oxide structures because the surface plasmon resonances of the gold particles can facilitate visible-light harvesting and induce strong localized electric field, which may enhance the activities for photocatalytic reactions, such as degradation of organic pollutants and water reduction for hydrogen generation.² However, most of previous studies on the plasmon-enhanced photocatalytic activity, in particular hydrogen generation from water reduction, were based on irradiation of “visible-light” with $\lambda > 400$ nm or 420 nm. When this wide-range irradiation can also induce slight excitation of the metal oxide structures, it becomes very difficult to differentiate between the multiple effects including 1) electron-sink effect as electron transfer from excited metal oxides to contacted metal particles;³ 2) resonant energy transfer between gold particles and metal oxides;^{2a,2f,4} 3) injection of hot surface electrons of plasmonic nanoparticles into conduction band of contacted metal oxides.^{2a,2e,4a,5} Although some researchers have clearly demonstrated that individual plasmon excitation of gold particles can induce certain photocatalytic activities, the efficiency is extremely low as compared to that of excited metal oxides with contacted metal particles as electron sinks.

As we know, electrospinning is a remarkably simple, versatile, and effective technique to process polymer, polymer/inorganic hybrid, and inorganic materials into continuous one-dimensional nanofibers with controllable composition, diameter and porosity,

which provide a mean to bridge the dimensional and property gaps between nano- and macro-scale engineering materials and structures.⁶ As such, the functional electrospun nanofibers have received much attention in the fields of photovoltaics, chemical sensors, and photocatalysis.⁷

Herein, in this work, we demonstrate a direct evidence, but at a different new sight of plasmon enhancement on photocatalytic hydrogen generation by using dual-beam irradiation, a primary beam at 420 nm (excite defect/impurity states of TiO₂) and a secondary beam at 550 nm (excite Au SPR), over the rationally designed structures, Au and Pt nanoparticles co-decorated TiO₂ (denoted as Au/Pt/TiO₂) nanofibers. We observe significantly enhanced hydrogen generation at simultaneous dual-beam irradiation comparing to the result when each irradiation (420 or 550 nm) is independently used. Further fine control on the secondary beam wavelength indicates that the enhancement factor can be directly correlated with the plasmon absorption band of the Au NPs in the Au/Pt/TiO₂ nanofibers. Moreover, we find that even if the primary beam is replaced by 365 nm irradiation for TiO₂ bandgap excitation, the secondary SPR irradiation still can enhance the hydrogen generation. Further control experiments suggest that the hot plasmon electrons on gold are responsible to the enhanced photocatalytic activity, which may be magnified when TiO₂ is simultaneously excited. Our observations reveal a synergic effect between Au SPR and TiO₂ excitation, which may play important roles in the previous studies on plasmon-related photocatalytic and photoelectrochemical reactions with wide-range irradiation of UV-vis or visible light.

Experimental Section

Fabrication of Au/Pt/TiO₂ composite nanofibers:

The Au/Pt/TiO₂ composite nanofibers were prepared via electrospinning followed by post-calcination. Typically, 2.0 mL of tetrabutyl titanate (Ti(OC₄H₉)₄) and 15 mg of H₂AuCl₄ (0.75 at.% Au to Ti) were introduced into a mixture solution of acetic acid (2 mL) and ethanol (5 mL) under stirring. Then, 0.4 g of poly(vinyl pyrrolidone) (PVP) powder (Mn=1300K) were added into the above solution which was kept stirring for 6 h. Then 8 mg H₂PtCl₆·6H₂O (8 mg, 0.25 at.% Pt to Ti) was added into this solution which was kept stirring for another 3 h. This precursor solution of PVP/H₂AuCl₄/H₂PtCl₆/Ti(OC₄H₉)₄ was then transferred into a plastic syringe with a stainless steel needle (23-gauge) for electrospinning, in which the feeding rate was 2.0 mL·h⁻¹ with ~15 cm distance between the needle tip and the collector. By applying an electric voltage of 15 kV between the needle tip and the collector, the dense web of electrospun nanofibers of the PVP/H₂AuCl₄/H₂PtCl₆/Ti(OC₄H₉)₄ composite was generated. Finally, these nanofibers were calcined in air at 500 °C (ramp rate of 2 °C·min⁻¹) for 2 h. The final product, Au/Pt/TiO₂ composite nanofibers are denoted as Au_x/Pt_{1-x}/TiO₂ in which x is the molar concentration (%) of Au to Ti in the precursor solution. In this work, the Au₁/TiO₂, Au_{0.75}/Pt_{0.25}/TiO₂, Au_{0.5}/Pt_{0.5}/TiO₂, Au_{0.25}/Pt_{0.75}/TiO₂ and Pt₁/TiO₂ nanofibers were fabricated to investigate the photocatalytic activity for H₂ generation.

25 Characterization:

X-ray diffraction (XRD) tests were performed on a Shimadzu XRD-600 X-ray diffractometer with a Cu K α line of 0.1541 nm. The morphologies and structures of the products were investigated by Field emission scanning electron microscopy (FESEM; JSM-7600F) and transmission electron microscopy (TEM; JEOL JEM-2100). The elemental composition was analysed through Energy dispersive X-ray spectroscopy (EDS) attached on the SEM and TEM. X-ray photoelectron spectroscopy (XPS) measurement was implemented on a Thermo Scientific Theta probe XPS with monochromatized Al K (h ν =1486.7 eV) source. The binding energy values were calibrated with respect to C (1s) peak (284.6 eV). UV-vis diffuse reflectance spectra were collected on a Lambda 750 UV/Vis/NIR spectrophotometer (Perkin Elmer, USA).

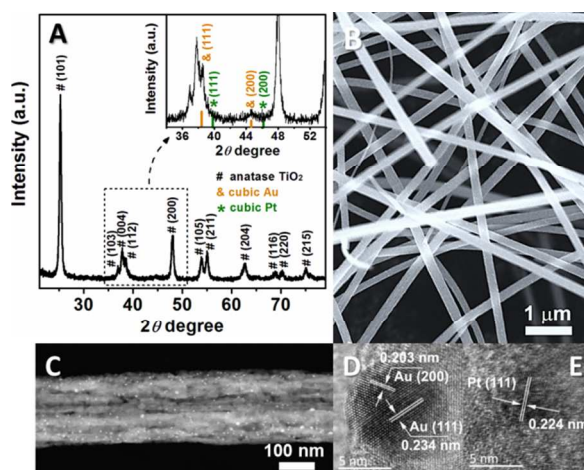
40 Photocatalytic hydrogen generation:

In a typical test, the prepared nanofibers (5 mg) were suspended in 10-mL aqueous solution of L-ascorbic acid (0.1 M, pH=4). This suspension was sealed in a quartz reactor (40 mL) with a rubber plug, and then purged with Ar gas for 30 min to drive away the residual oxygen. Then the reactor was exposed under a 300-W xenon lamp (MAX-302, Asahi Spectra Co. Ltd.) coupled with different bandpass filters (e.g. 420 \pm 10 or 365 \pm 10 nm). The light intensities for 420 \pm 10 and 365 \pm 10 nm are about 8 and 4 mW/cm², respectively. The secondary irradiation was implemented by using a 150-Watt Xe lamp (MAX-150, Asahi Spectra Co. Ltd.) coupled with different bandpass filters such as 520 \pm 5, 540 \pm 5, 560 \pm 5, 580 \pm 5, and 550 \pm 20 nm. The light intensities are about 1.5 mW/cm² for 520 \pm 5, 540 \pm 5, 560 \pm 5, and 580 \pm 5 nm, while the light intensity of 550 \pm 20 nm is about 20 mW/cm². The gas product composition from the upper space above the liquid suspension in the quartz reactor was periodically analyzed by an Agilent 7890A gas chromatograph (GC) equipped

with a thermal conductivity detector (TCD).

Results and Discussion

The TiO₂ nanofiber containing 0.75% Au and 0.25 % Pt (mole fraction), denoted as Au_{0.75}/Pt_{0.25}/TiO₂, were fabricated via electrospinning. In this designed structure, the decorated Au NPs would provide the SPR effect, while the minor portion of Pt NPs would serve as effective electron-sinks with activation effect for H₂ evolution. The X-ray diffraction (XRD) pattern (Figure 1A) shows the signals of anatase TiO₂ (JCPDS, no. 21-1272) and cubic-phase Au (JCPDS, no. 04-0784) nanocrystals. But the signal of Pt nanocrystals was hardly observable due to the very low concentration of Pt in the sample. Note that the Au peaks in the XRD pattern did not show any shift comparing to the standard JCPDS pattern, suggesting no Au-Pt alloy formation which was further confirmed by the X-ray photoelectron spectroscopy (XPS) (Figure S1).



75 **Fig. 1** (A) XRD pattern, (B) SEM image, and (C) dark-field STEM image of the Au_{0.75}/Pt_{0.25}/TiO₂ nanofibers; HRTEM images of (D) Au NPs and (E) Pt NPs in the Au_{0.75}/Pt_{0.25}/TiO₂ nanofibers.

The scanning electron microscopy (SEM) image (Figure 1B) shows that the fabricated nanofibers have a mean diameter of ~190 nm with lengths up to several micrometers. The EDS analysis confirms that the element contents of Au and Pt in the as-electrospun Au/Pt/TiO₂ nanofibers are very close to the theoretical value in the electrospun precursor solution (Figure S2). The dark-field scanning transmission electron microscopy (TEM) clearly indicates the decoration of metal NPs with average size of 7.2 nm in the nanofiber (Figure S2). The EDS mapping images, shown in Figure S2, reveal a well-dispersed distribution of the metal (Au or Pt) NPs in the nanofibers. Although it is difficult to differentiate the composition of every particles, in the high-resolution TEM (HRTEM) images (Figure 1D and 1E) we can clearly observe the interplanar distances of 0.234, 0.203, and 0.224 nm, corresponding to the lattice spacing of the Au (111), Au (200), and Pt (111) planes, respectively. These observations suggest co-existence of metallic Au and Pt NPs in the Au/Pt/TiO₂ nanofibers. Nevertheless, we note that some Pt NPs as observed in HRTEM have very small size (<5 nm), and not be distinguishable in the dark-field TEM image (Figure 1C).

The UV-Vis absorption spectrum of Au_{0.75}/Pt_{0.25}/TiO₂ nanofibers is shown in Figure 2. The pure TiO₂ nanofibers and

Pt₁/TiO₂ nanofibers (containing 1% Pt in mole fraction), were also prepared through similar electrospinning methods and used for comparison. The intense UV absorption band below 400 nm could be assigned to the intrinsic bandgap absorption of anatase TiO₂ (E_g: ~3.2 eV). Comparing with pure TiO₂ nanofibers, the Au_{0.75}/Pt_{0.25}/TiO₂ nanofibers exhibit a clear absorption band centered at ~540 nm which could be attributed to the SPR of embedded Au NPs. Note that this SPR peak wavelength is relatively red-shifted as compared to that of similar sized Au NPs due to the high refractive index of the anatase TiO₂ matrix (n=2.49).⁸ However, this Au SPR peak (~540 nm) is blue-shifted as compared to the SPR peak of the Au₁/TiO₂ nanofibers (~590 nm) (Figure S3), which might be ascribed to the existence of Pt NPs with more negative dielectric function and the relative larger size of Au NPs in the Au₁/TiO₂ nanofibers.⁹ The SPR of Pt NPs is not observed due to the high imaginary part of the dielectric function of Pt.⁹ In addition, the weak absorption of Pt₁/TiO₂ nanofibers in the visible range might be attributed to defects/impurities induced by the Pt²⁺ and Pt⁴⁺ states in the TiO₂ nanofibers as revealed by XPS analyses (Figure S1).¹⁰

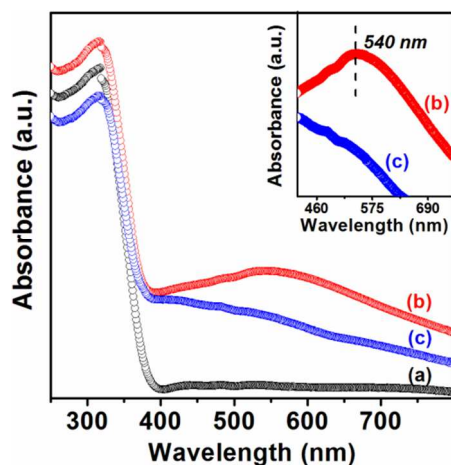


Fig. 2 UV-Vis absorption spectra of the (a) pure TiO₂, (b) Au_{0.75}/Pt_{0.25}/TiO₂, and (c) Pt₁/TiO₂ nanofibers, which are converted from diffuse reflectance spectra by means of the Kubelka-Munk function.

The photocatalytic H₂ generation tests were conducted in aqueous solution of L-ascorbic acid (0.1 M, pH=4.0) as the sacrificial reagent to quench the photogenerated holes. As shown in Figure 3A, the Au_{0.75}/Pt_{0.25}/TiO₂ nanofibers show steady H₂ evolution with a rate of 0.043 μmol·h⁻¹ under irradiation at 420±10 nm. This result suggests that the defect/impurity states of the TiO₂ nanofiber can be excited by the visible light irradiation for proton reduction in the presence of Au and Pt NPs as co-catalysts, which can act as electron sinks to hold the electrons from the excitation of TiO₂ defect/impurity states and retard the recombination process of photogenerated charge carriers. In contrast, there was no H₂ evolution for the Au_{0.75}/Pt_{0.25}/TiO₂ nanofibers under irradiation at 550±20 nm which could strongly excite the SPR of Au NPs in the nanofibers, suggesting that plasmon-excited hot electrons could not directly induce activities for proton reduction under this condition, and also this 550±20 nm light could not excite the TiO₂ defect/impurity states for photocatalytic H₂ generation.

However, to our surprise, when these two irradiations (420±10

nm and 550±20 nm) were implemented simultaneously for the photocatalytic test, the H₂ evolution rate of the Au_{0.75}/Pt_{0.25}/TiO₂ nanofibers could reach 0.108 μmol·h⁻¹, which is about 2.5 times higher than the rate under single irradiation at 420±10 nm. Interestingly, this phenomenon can be also observed on the Au/Pt/TiO₂ nanofibers with different Au to Pt mole ratios (Figure S4). Among them, the Au_{0.75}/Pt_{0.25}/TiO₂ nanofibers show the optimal enhancement factor when the secondary irradiation at 550 nm is introduced to simultaneously excite Au SPR due to the higher content of Au in the nanofibers. These results imply that the secondary excitation at 550±20 nm for Au SPR excitation could significantly enhance the photocatalytic activity driven by the 420 nm excitation of TiO₂ defect/impurity states that are intrinsically inactive to the 550±20 nm light. In comparison, for the Pt₁/TiO₂ nanofiber, the dual-beam irradiation led to the same H₂ generation rate (0.062 μmol·h⁻¹) with single irradiation at 420±10 nm, suggesting no enhancement on the photocatalytic activity from the secondary 550 nm irradiation. This observation demonstrates that the SPR of Au NPs in the Au/Pt/TiO₂ nanofibers is responsible to the enhanced photocatalytic H₂ generation upon the secondary irradiation at 550±20 nm.

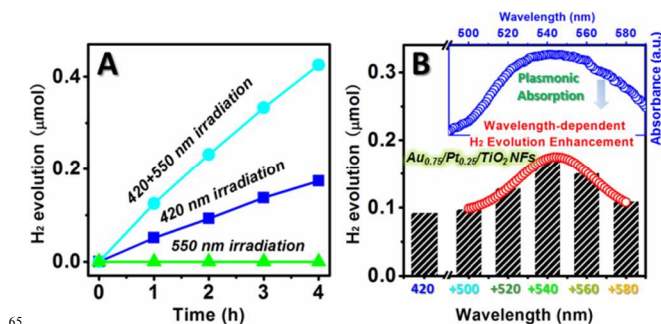


Fig. 3 (A) The photocatalytic H₂ evolution over the Au_{0.75}/Pt_{0.25}/TiO₂ nanofibers under irradiation at single 420±10 nm, single 550±20 nm, and both 420±10 nm and 550±20 nm; (B) H₂ evolution amount of the Au_{0.75}/Pt_{0.25}/TiO₂ nanofibers versus the irradiation wavelength after 2 h irradiation. The inset shows the plasmonic absorption of Au NPs in the Au_{0.75}/Pt_{0.25}/TiO₂ nanofibers, which is derived from Figure 2 curve (b).

In order to clarify the enhancement effect of plasmon excitation, we carry out comparison experiments by using different secondary irradiation (with the same intensity of 1.5 mW/cm²) at 520±5, 540±5, 560±5, and 580±5 nm, respectively. This wavelength selection is based on the Au SPR band (~540 nm) according to the absorption spectrum (Figure 2). As shown in Figure 3B, all different secondary irradiation wavelengths led to certain enhancement on the H₂ generation rate, and the enhancement factor exhibits strong dependence on the secondary irradiation wavelength which correlates well with the plasmon absorption of Au NPs (Figure 3B inset) in the Au_{0.75}/Pt_{0.25}/TiO₂ nanofibers. The irradiation at 540±5 nm provides the highest enhancement factor (1.9x) on the photocatalytic activity of H₂ evolution driven by the 420±10 nm irradiation. These results unambiguously demonstrate the direct evidence of SPR-enhanced photocatalytic H₂ generation on the Au/Pt/TiO₂ nanofibers.

To gain further understanding on how the SPR enhances H₂ generation under the present experimental conditions with dual-beam irradiation, we would like to firstly separate the electron-sink effect from the Au NPs in the Au_{0.75}/Pt_{0.25}/TiO₂ nanofibers. Since Pt has lower H₂ evolution overpotential than Au, Pt NPs are

known as better electron sinks than Au NPs for H₂ evolution. Consistently, the control sample, Au₁/TiO₂ nanofiber (containing 1% mole fraction of Au) showed 24 times lower H₂ evolution rate (0.0018 μmol·h⁻¹) than the Au_{0.75}/Pt_{0.25}/TiO₂ nanofibers under irradiation at 420±10 nm (Figure S5). This result suggests that in the Au/Pt/TiO₂ nanofibers, the proton reduction occurs mainly on the Pt NP surfaces, and Au NPs play very minor roles as electron sink in the present studies. Therefore, in the following discussion, we only consider hydrogen evolution on Pt NP surfaces.

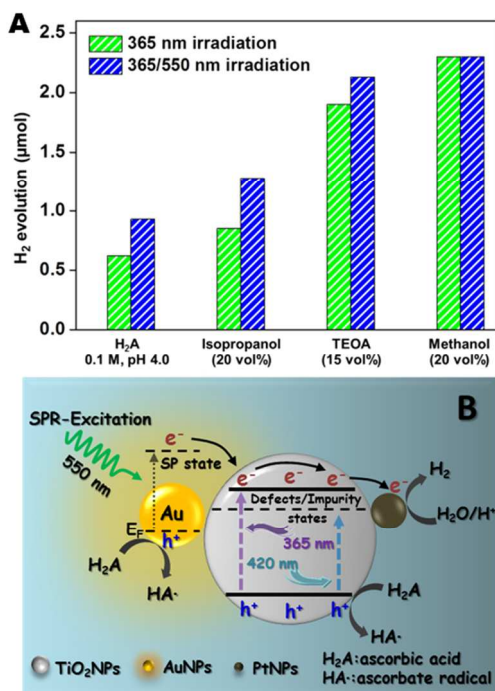


Fig. 4 Caption(A) H₂ evolution amount for the Au_{0.75}/Pt_{0.25}/TiO₂ nanofibers versus the irradiation wavelength after 2 h irradiation using L-ascorbic acid (H₂A), isopropanol, triethanolamine (TEOA), and methanol as the sacrificial agents in 10 mL aqueous solution, respectively; (B) Schematic diagram showing the proposed principle of plasmon enhanced photocatalytic hydrogen generation on the Au_{0.75}/Pt_{0.25}/TiO₂ nanofibers. The key point is only when TiO₂ is excited (by 420 nm or 365 nm), the hot plasmon electrons of Au NPs can easily transport through TiO₂ to nearby Pt NPs, leading to enhanced H₂ generation.

In our studies, the two irradiation beams play separate roles. The 420 nm irradiation creates TiO₂ excitons that separate at TiO₂-Pt interface to reduce water for H₂ evolution, but hardly excites Au SPR. The 550 nm irradiation can excite Au SPR, but can not excite the TiO₂ defect/impurity states for H₂ generation. Therefore, the resonance energy transfer between Au and TiO₂ is not applicable in our observed SPR-enhanced activity. Interestingly, if the primary excitation is set at 365±10 nm, which can induce bandgap excitation of TiO₂, a secondary excitation at 550±20 nm still can lead to enhanced photocatalytic activity for H₂ generation with factor of 1.5x (Figure 4A), though it is lower than that (2.5x) in case of primary excitation at 420±10 nm. Further, we carried out similar photocatalytic studies with different sacrificial agents such as isopropanol, triethanolamine (TEOA), and methanol. The individual irradiation at 550±20 nm could not lead to observable H₂ generation for methanol and TEOA, while trace amount of H₂ was observed (~0.002 μmol after 2-hour irradiation) when using isopropanol. By comparing

the H₂ generation rate between single irradiation (365±10 nm) and dual-beam irradiation (365±10 nm and 550±20 nm), we observed an enhancement factor of 1.12 and 1.51 for TEOA and isopropanol, respectively, but no enhancement was observed for methanol.

The different enhancement factor suggests that the strong localized electric field by SPR excitation may not be the dominating factor on the enhanced H₂ generation. Otherwise, one would expect the same enhancement factor no matter what sacrificial agent is used because the SPR-induced local electric field at the Au/TiO₂ interfaces is essentially identical under the same 550 nm irradiation with no dependence on the sacrificial agent. Consequently, the possible explanation on the enhanced H₂ generation activity would rely on the hot plasmon electrons. However, we note that in the presence of the primary irradiation at 365 nm, the additional H₂ generation activity induced by the secondary 550 nm irradiation is far beyond H₂ evolution induced by the individual 550 nm irradiation that hardly led to H₂ generation. Thus the question is converted to why the hot plasmon electrons can not induce H₂ generation if TiO₂ is not excited, but can induce apparent H₂ generation when TiO₂ is excited.

A recent study by Kominami et al. suggests that the hot electrons by SPR excitation might be able to transport through TiO₂ nanocrystals to the nearby Pt NPs for reactions.¹¹ If this is true, the conductivity of TiO₂ becomes critical to the lifetime of the hot plasmon electrons, which is consistent with our observation. It is known that the photoexcited semiconductor exhibits higher conductivity because more charge carriers are created in the structure by the excitation.¹² In our studies, when dual-beam irradiation is used, both TiO₂ matrix and Au SPR are excited, the hot plasmon electrons are able to rapidly transport through the contacted TiO₂ nanocrystal to the nearby Pt NPs for proton reduction into H₂ due to the high conductivity of excited TiO₂. In comparison, if the individual 550 nm light is used, it only excites Au SPR, the hot electrons can hardly pass through TiO₂ crystal to reach the near Pt NPs due to the low conductivity of un-excited TiO₂, thus almost no H₂ generation was observed. This explanation, as illustrated in figure 4B, also agrees with the observed dependence of enhancement factor on the sacrificial agent and its capability of quenching the photogenerated holes on gold. Similar dependence of photocatalytic activity on the hole scavenger agent was also reported by Berr et al.¹³ In our case, the trend of enhancement factor would critically depend on the oxidation reaction on gold surface rather than the redox potential of different sacrificial agents. Even though methanol can efficiently quench the holes on TiO₂ upon 365 nm excitation, it may be hardly oxidized by the holes of gold under SPR excitation, thus no enhanced H₂ generation was observed under dual-beam irradiation in case of methanol as electron donor. More details on the effect of sacrificial agents and their reaction kinetics on gold surfaces are under investigation.

90 Conclusion

We have demonstrated direct evidence of SPR-enhanced photocatalytic hydrogen evolution by combining two separate irradiations on Au and Pt NPs co-decorated TiO₂ nanofibers. The enhancement factor is directly correlated with the plasmon

absorption band of the Au NPs in the nanofibers. Further studies suggest that the hot plasmon electrons are responsible to the enhanced H₂ generation when the matrix of TiO₂ nanofibers is simultaneously excited. Importantly, this work reveals a synergic effect between Au SPR and TiO₂ excitation. We believe that similar synergic effect may also exist and play important roles in other plasmon-related photocatalytic reactions and photoelectrochemical systems under wide range irradiation that excites both metal SPR and semiconductors. Our studies also demonstrate that by introducing SPR excitation at relatively low energy photons, one can enhance the photocatalytic efficiency of semiconductors excited by high energy photons (UV- or blue-light), which allows for more effective utilization of the wide range of solar irradiation.

Acknowledgements

This work is financially supported by NTU seed funding for Solar Fuels Laboratory, MOE AcRF-Tier1 RG 44/11, MOE AcRF-Tier 2 (MOE2012-T2-2-041, ARC 5/13), and CRP (NRF-CRP5-2009-04) from NRF Singapore.

Notes and references

^a School of Physics and Materials Engineering, Dalian Nationalities University, Dalian, 116600, PR China.

^b Solar Fuels Laboratory, School of Materials Science and Engineering, Nanyang Technological University, 50 Nanyang Avenue, Singapore 639798, Singapore. Fax: +65 6790 9081; Tel: +65 6790 6180; E-mail: cxue@ntu.edu.sg

^c Institute of Materials Research and Engineering A* STAR, 3 Research Link, 117602, Singapore.

† Electronic Supplementary Information (ESI) available: [XPS, TEM, EDS, and photocatalytic H₂ evolution data]. See DOI: 10.1039/b000000x/

- 1 a) D. Ravelli, D. Dondi, M. Fagnoni and A. Albini, *Chem. Soc. Rev.*, 2009, **38**, 1999; b) J. A. Turner, *Science*, 1999, **285**, 687; c) S. U. M. Khan, M. Al-Shahry and W. B. Ingler Jr, *Science*, 2002, **297**, 2243; d) H. Yoneyama, Y. Yamashita and H. Tamura, *Nature*, 1979, **282**, 817; e) Z. Y. Yin, Z. Wang, Y. P. Du, X. Y. Qi, Y. Z. Huang, C. Xue and H. Zhang, *Adv. Mater.* 2012, **24**, 5374; f) K. Maeda and K. Domen, *J. Phys. Chem. Lett.*, 2010, **1**, 2655.
- 2 a) S. Linic, P. Christopher and D. B. Ingram, *Nature Mater.* 2011, **10**, 911; b) P. Wang, B. Huang, X. Qin, X. Zhang, Y. Dai, J. Wei and M. Whangbo, *Angew. Chem. Int. Ed.* 2008, **47**, 7931; c) Y. Ide, M. Matsuoka and M. Ogawa, *J. Am. Chem. Soc.*, 2010, **132**, 16762; d) Z. Y. Zhang, Z. Wang, S. W. Cao and C. Xue, *J. Phys. Chem. C* 2013, **117**, 25939; e) Y. Tian and T. Tatsuma, *J. Am. Chem. Soc.*, 2005, **127**, 7632; f) Z. Liu, W. Hou, P. Pavaskar, M. Aykol and S. B. Cronin, *Nano Lett.*, 2011, **11**, 1111; g) Z. W. Seh, S. Liu, M. Low, S. Zhang, Z. Liu, A. Mlayah and M. Han, *Adv. Mater.* 2012, **24**, 2310; h) L. Liu, S. Ouyang and J. Ye, *Angew. Chem. Int. Ed.*, 2013, **52**, 6689; i) Y. Pu, G. Wang, K. Chang, Y. Ling, Y. Lin, B. C. Fitzmorris, C. Liu, X. Lu, Y. Tong, J. Z. Zhang, Y. Hsu and Y. Li, *Nano Lett.*, 2013, **13**, 3817.
- 3 a) M. Murdoch, G. I. N. Waterhouse, M. A. Nadeem, J. B. Metson, M. A. Keane, R. F. Howe, J. Llorca and H. Idriss, *Nature Chem.* 2011, **3**, 489; b) Z. Zheng, B. Huang, X. Qin, X. Zhang, Y. Dai and M. Whangbo, *J. Mater. Chem.*, 2011, **21**, 9079; c) Y. Pan, S. Deng, L. Polavarapu, N. Gao, P. Yuan, C. H. Sow and Q. Xu, *Langmuir*, 2012, **28**, 12304.
- 4 a) W. Hou and S. B. Cronin, *Adv. Funct. Mater.*, 2012, **23**, 1612; b) S. K. Cushing, J. Li, F. Meng, T. R. Senty, S. Suri, M. Zhi, M. Li, A. D. Bristow and N. Wu, *J. Am. Chem. Soc.*, 2012, **134**, 15033; c) D. B. Ingram and S. Linic, *J. Am. Chem. Soc.*, 2011, **133**, 5202; d) S. W. Cao, Z. Yin, J. Barber, F. Boey, S. C. J. Loo and C. Xue, *ACS Appl. Mater. Interfaces*, 2012, **4**, 418; e) H. Wang, T. You, W. Shi, J. Li and L. Guo, *J. Phys. Chem. C*, 2012, **116**, 6490.
- 5 a) W. Hou, W. H. Hung, P. Pavaskar, A. Goepfert, M. Aykol and S. B. Cronin, *ACS Catal.*, 2011, **1**, 929; b) S. Mubeen, J. Lee, N. Singh, S. Krämer, G. D. Stucky and M. Moskovits, *Nat. Nanotechnol.*, 2013, **8**, 247; c) S. Mubeen, G. Hernandez-Sosa, D. Moses, J. Lee and M. Moskovits, *Nano Lett.*, 2011, **11**, 5548; d) M. M. Shahjamali, M. Bosman, S. W. Cao, X. Huang, S. Saadat, E. Martinsson, D. Aili, Y. Y. Tay, B. Liedberg, S. C. J. Loo, H. Zhang, F. Boey and C. Xue, *Adv. Funct. Mater.* 2012, **22**, 849; e) J. Lee, S. Mubeen, X. Ji, G. D. Stucky and M. Moskovits, *Nano Lett.*, 2012, **12**, 5014.
- 6 a) D. He, B. Hu, Q.-F. Yao, K. Wang and S.-H. Yu, *ACS Nano*, 2009, **3**, 3993; b) C.-L. Zhang, K.-P. Lv, H.-P. Cong and S.-H. Yu, *Small*, 2012, **8**, 648; c) C.-L. Zhang, K.-P. Lv, N.-Y. Hu, L. Yu, X.-F. Ren, S.-L. Liu, S.-H. Yu, *Small*, 2012, **8**, 2936; d) C.-L. Zhang, K.-P. Lv, H.-T. Huang, H.-P. Cong and S.-H. Yu, *Nanoscale*, 2012, **4**, 5348.
- 7 a) S. K. Choi, S. Kim, S. K. Lim, H. Park, *J. Phys. Chem. C*, 2010, **114**, 16475; b) Y. Chen, Y. Chang, J. Huang, I. Chen and C. Kuo, *J. Phys. Chem. C*, 2012, **116**, 3857; c) H. Wu, Y. Sun, D. Lin, R. Zhang, C. Zhang and W. Pan, *Adv. Mater.*, 2009, **21**, 227; d) I. Kim and A. Rothschild, *Polym. Adv. Technol.*, 2011, **22**, 318.
- 8 a) J. Fang, S. Cao, Z. Wang, M. M. Shahjamali, S. C. J. Loo, J. Barber and C. Xue, *Int. J. hydrogen Energy*, 2012, **37**, 17853; b) E. Kowalska, O. O. P. Mahaney and R. Abe, B. Ohtani, *Phys. Chem. Chem. Phys.*, 2010, **12**, 2344.
- 9 a) E. D. Gaspera, M. Bersani, G. Mattei, T. Nguyen, P. Mulvaney and A. Martucci, *Nanoscale*, 2012, **4**, 5972; b) L. M. Liz-Marzán and A. P. Philipse, *J. Phys. Chem.*, 1995, **99**, 15120.
- 10 a) S. Kim, S. Hwang and W. Choi, *J. Phys. Chem. B*, 2005, **109**, 24260; b) Y. Ishibai, J. Sato, T. Nishikawa and S. Miyagishi, *Appl. Catal. B: Environ.*, 2008, **79**, 117; c) Y. Chen, M. Franzreb, R. Lin, L. Chen, C. Chang, Y. Yu and P. Chiang, *Ind. Eng. Chem. Res.*, 2009, **48**, 7616; d) B. K. Vijayan, N. M. Dimitrijevic, J. Wu and K. A. Gray, *J. Phys. Chem. C*, 2010, **114**, 21262.
- 11 A. Tanaka, S. Sakaguchi, K. Hashimoto and H. Kominami, *ACS Catal.*, 2013, **3**, 79.
- 12 a) N. K. Subbaiyan, C. A. Wijesinghe and F. D'Souza, *J. Am. Chem. Soc.*, 2009, **131**, 14646; b) P. Atienzar, T. Ishwara, B. N. Illy, M. P. Ryan, B. C. O'Regan, J. R. Durrant and J. Nelson, *J. Phys. Chem. Lett.*, 2010, **1**, 708; c) Y. An, L. Tang, X. Jiang, H. Chen, M. Yang, L. Jin, S. Zhang, C. Wang and W. Zhang, *Chem. Eur. J.*, 2010, **16**, 14439; d) Y. Nishijima, K. Ueno, Y. Yokota, K. Murakoshi and H. Misawa, *J. Phys. Chem. Lett.*, 2010, **1**, 2031; e) D. Wang, T. Hu, L. Hu, B. Yu, Y. Xia, F. Zhou and W. Liu, *Adv. Funct. Mater.*, 2009, **19**, 1930.
- 13 M. J. Berr, P. Wagner, S. Fischbach, A. Vaneski, J. Schneider, A. S. Susha, A. L. Rogach, F. Jaockel and J. Feldmann, *Appl. Phys. Lett.*, 2012, **100**, 223903.